Optimized Heterointerface of BiVO$_4$/C$_3$N$_4$ by Co Single Atom and F-doping for Boosting Photoelectrochemical water splitting

Sihong Xia[#], Fenghua Xu[#] and Baicheng Weng*

Department of Chemistry and Chemical Engineering, Central South University, Changsha 410083, China

*E-mail: bcweng@mail.csu.edu.cn

[#] *These authors contribute equally to this work.*

Experimental section

Preparation of g-C$_3$N$_4$ and Co:C$_3$N$_4$. *g*-C$_3$N$_4$: *g*-C$_3$N$_4$ was prepared by a thermal polymerization method. Briefly, 20 g dicyandiamide was placed in the center of a muffle furnace and heated to 550 °C for 4 h, with a ramping rate of 5 °C min^{-1}. Then the *g*-C$_3$N$_4$ powder was obtained after the sample was cooled down naturally. 9 grams of *g*-C$_3$N$_4$ powder was dispersed in 90 mL anhydrous H$_2$SO$_4$ and stirred for 1 h, then 90 mL of deionized (DI) water was dropped to the mixture to obtain a clear solution. Then 300 mL ethanol was added to the clear solution and stirred for 18 h. The precipitates were washed with DI water and vacuum dried at 60°C to obtain **g-C$_3$N$_4$ nanosheets.**

Co:C$_3$N$_4$: Varied amount of Co(NO$_3$)$_2$ powder with molar ratios of 5:1, 7:1 and 10:1 (Co:C$_3$N$_4$) was dissolved in 5 mL DI water to obtain a clear solution, and then 1 g *g*-C$_3$N$_4$ nanosheets were added to the solution and stirred for 2 min. Then the mixture was filtered and put into a tube furnace at 130 °C. The powder was then heated to 550°C at a heating rate of 100 °C min^{-1} to kept at this temperature for 6 h. After cooling down to room temperature, the obtain sample was washed with 0.1 M HNO$_3$ and DI water.

Preparation of BiVO$_4$ and F:BiVO$_4$. 3.32 g KI was dissolved in 50 mL DI water and the pH was adjusted to 1.7 by HNO$_3$, then 0.9702 g Bi(NO$_3$)$_3$ was added into the solution under stirring until it was completely dissolved. Then, 20 mL of absolute ethanol (100%) containing 0.52 g p-benzoquinone (97%, Aladdin) was mixed into the above solution and vigorously stirred for several minutes. Cathodic deposition of BiOI (1×1 cm^2) was performed potentiostatically in the final solution at −0.1 V vs. Ag/AgCl at room temperature for 200 s. The second step was the conversion of BiOI to BiVO$_4$. 0.5678 M vanadyl acetylacetonate was impregnated on BiOI electrodes (50 μL cm^{-1}) and then annealed in air at 450 °C for 2 h with ramping rate of 2 °C min^{-1}. Then the BiVO$_4$ electrodes were soaked in 1 M NaOH solution for 1 h with gently stirring to remove the excess V$_2$O$_5$, and then rinsed by deionizer water. The preparing procedure for F-doping is similar to that of BiVO$_4$, expect 20 μL, 40 μL, and 60 μL NH$_4$F solution was added with vanadyl acetylacetonate. The NH$_4$F solution was prepared by dissolving 0.0082 g NH$_4$F into 2 ml DI water.

Preparation of heterojunctions. 100 mg C$_3$N$_4$ or Co: C$_3$N$_4$ was dispersed in 20 mL DI water, and the suspension was spin coated onto the substrate surface at 2,500 rpm for 1 min. After repeating several times, the as-obtained samples were thermally annealed in air at 350 °C in air for 1 h at a ramping rate of 10 °C min^{-1}.

β-FeOOH co-catalysts loading. β-FeOOH was prepared by electrochemical photodeposition in a 0.1 M $FeSO_4$ aqueous solution at 0.25 V vs. Ag/AgCl for 2 min under AM 1.5 G illumination.

Material characterizations

The X-ray absorption spectra (XAS) including X-ray absorption near-edge structure (XANES) and extended X-ray absorption fine structure (EXAFS) of the samples at Co K-edge were collected at the Shanghai Synchrotron Radiation Facility. A double Si(111)-crystal monochromator was used for energy selection. Co foil was employed to calibrate the energy. The spectra were collected at transmission mode at room temperature. The Athena software package was used to analyze the data. The crystal phases were determined by a powder X-ray diffractometer (XRD, Rigaku Ultima III, Japan) operated at 20 kV and 40 mA with Cu-Ka radiation. The surface morphology was examined using scanning electron microscopy (SEM, FEI Nova Nano SEM 230, USA). Elemental compositions were measured by energy dispersive X-ray spectroscopy (EDX) (Oxford Instruments) at 200 kV and calibrated with standard Cu and Co target before testing. Scanning transmission electron microscopy (STEM, Tecnai TF-30, operated at 300 kV) were conducted for elemental mapping. Diffused reflectance spectrum was scanned using a UV-vis spectrophotometer (UV-2500, Shimadzu Co., Japan) and transformed into absorption spectrum according to the Kubelka–Munk relationship. Aberration-corrected high-angle annular dark-field scanning transmission electron microscopy (AC-HAADF-STEM) images and associated energy-dispersive x-ray energy spectra (EDX) were recorded on a Themis Z equipped with an FEI Super X-EDX system and a double-corrected FEI Titan Themis TEM. Valence band position and Fermi level were determined by X-ray Photoelectron Spectroscopy (XPS) and Ultroviolet Photoelectron Spectroscopy (UPS, Thermo Fisher Scientific ESCALab250). The light intensity was calibrated using silicon reference solar cells (Oriel, 91150 V).

Photoelectrochemical measurements

Photoelectrochemical tests were composed of a standard three-electrode configuration in a 0.5 M KBi electrolyte (pH = 9.3). The counter and the reference electrodes were the platinum wire and the Ag/AgCl reference electrode, respectively. The electrolyte was stirred and purged with Ar gas before measurements. The photoelectrodes with an exposure area of 1 cm^2 were illuminated under AM 1.5G light (100 mW cm^{-2}, 300 W Xe lamp). The wavelength dependence of incident-photon-to-current conversion efficiency (IPCE) was measured under monochromatic irradiation from a 300 W Xe lamp equipped with bandpass filters. The applied bias photon-to-current efficiency (ABPE) was calculated from the two-electrode current-potential curves under AM 1.5G light. The electrochemical impedance spectra (EIS) tests were measured by AC impedance spectroscopy at the frequency ranges 106 to 0.1 Hz. The potentials were displayed versus reversible hydrogen electrode (RHE) by: $E_{(RHE)} = E_{(Ag/AgCl)} + 0.197 + 0.0591 \times pH$.

Oxygen evolution reaction (OER) kinetics tests

The OER activity was examined using the conventional Rotating disk electrode (RDE) technique. The RDE system comprised a rotation controller (Pine, UK), water-jacketed glass cell equipped with a Luggin capillary and reversible hydrogen reference electrode (RHE), platinum wire and disk counter electrode, and catalyst-coated working electrode. The working electrode was polytetrafluoroethylene (PTFE)-insulated polycrystalline gold disk electrode (6 mm diameter, 0.283 cm2), which was polished with emery paper (#2000) and ultrasonically cleaned in highly purified water (Puric-ω, Organo). The OER activity was evaluated anodically by LSV at 5 mV s^{-1} and 1600 rpm.

Computational details

All calculations were conducted by density functional theory (DFT) methods, as implemented in the Vienna ab initio simulation package (VASP).[1-5] Briefly, the core electrons were described by the projector augmented wave (PAW) pseudopotentials. The generalized gradient approximation (GGA) potential was used to tackle the exchange-correlation interactions of electrons. The energy cutoff for the plane-wave basis set was 520 eV for $BiVO_4$ and $F:BiVO_4$, and 450 eV for $g-C_3N_4$ and $Co:C_3N_4$. The Monkhorst-Pack k-point samplings were set to $10 \times 10 \times 4$ for $BiVO_4$ and $F:BiVO_4$, and $3 \times 1 \times 1$ for monolayer $g-C_3N_4$ and $Co:C_3N_4$. A vacuum region of 20 Å was added above monolayer $g-C_3N_4$ and $Co:C_3N_4$ to minimize the interactions between neighboring systems. Fixed cell parameters and model structures were optimized using the convergence criteria of 10^{-5} eV for the electronic energy and 0.01 eV/Å for the residual forces on each atom. All the atoms were allowed to move during the geometrical optimization. All calculations were taken into account the spin polarization. For $BiVO_4$ calculation, Since the GGA-PBE method generally underestimates the band gap, it was corrected using the DFT + U approach. The calculated band gap was 2.4 eV for U = 4.6 eV, which is consistent with previous reports.[6]

Supporting Figures and Table:
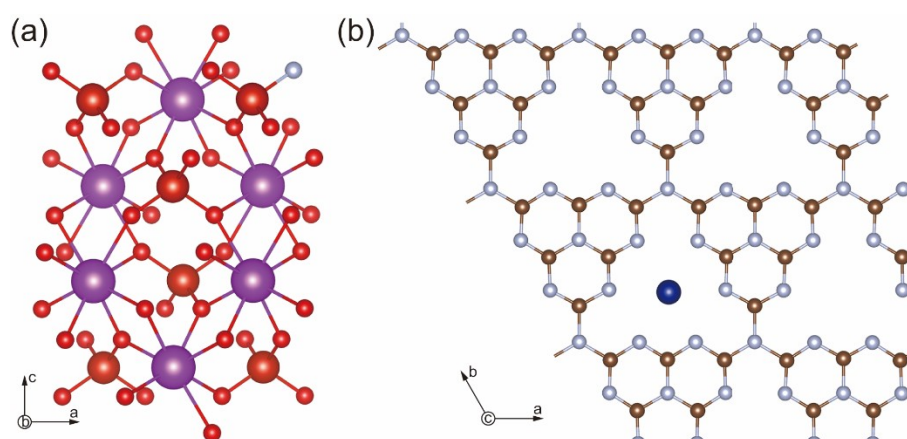
Figure S1. Built structural models of F-doped $BiVO_4$ (a), and $Co:C_3N_4$.

The contents of F in $F:BiVO_4$ and Co in $Co:C_3N_4$ are 4.1 at.% and 5.1 wt.%, respectively. the measured doping level of F is slightly lower than that of calculated model, while the content of Co is slightly higher. The calculated models are actually built according to the experimental measurements and we used different content to avoid building extremely large supercells.
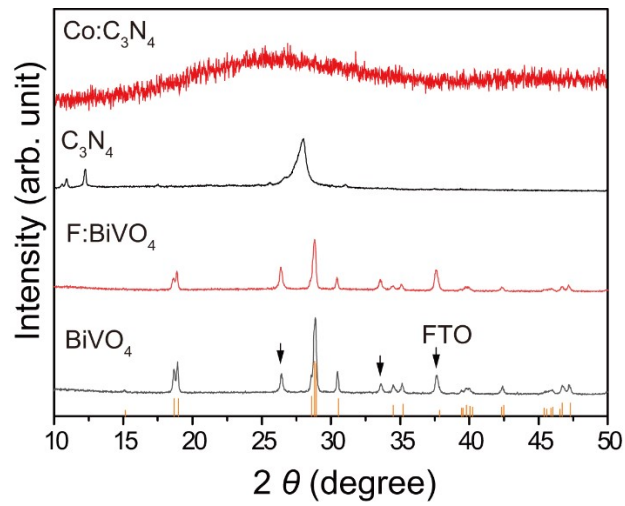
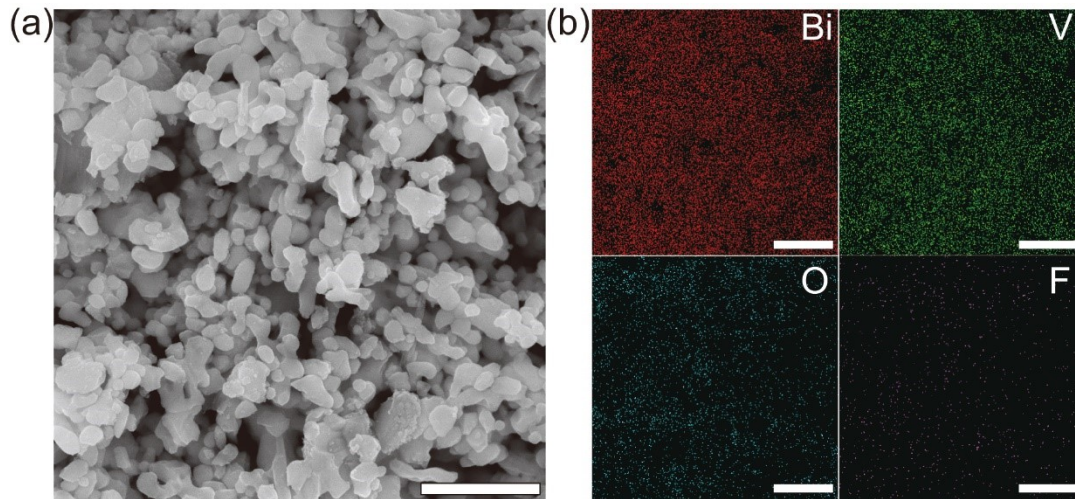**Figure S2.** XRD patterns of $BiVO_4$, C_3N_4, $F:BiVO_4$ and $Co:C_3N_4$.

Figure S3. (a) SEM image and (b) EDX elemental mapping of $F:BiVO_4$.
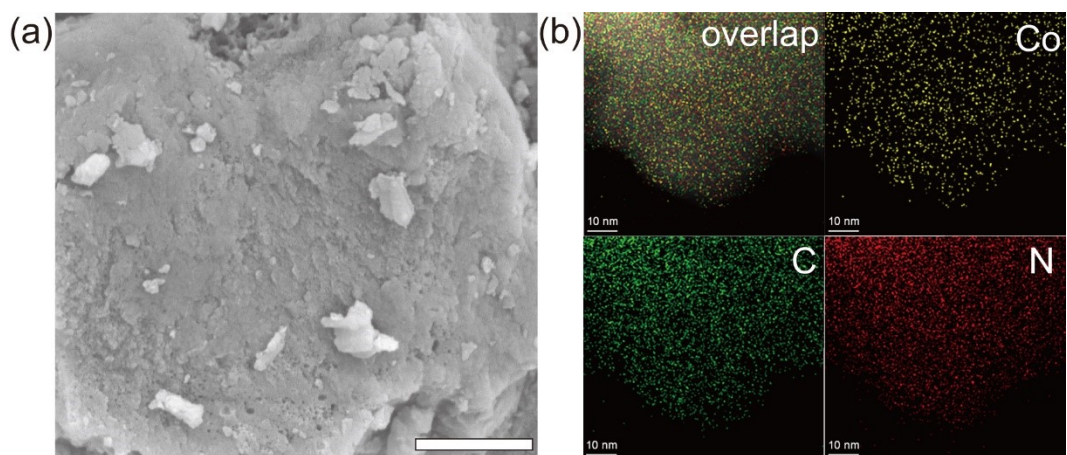

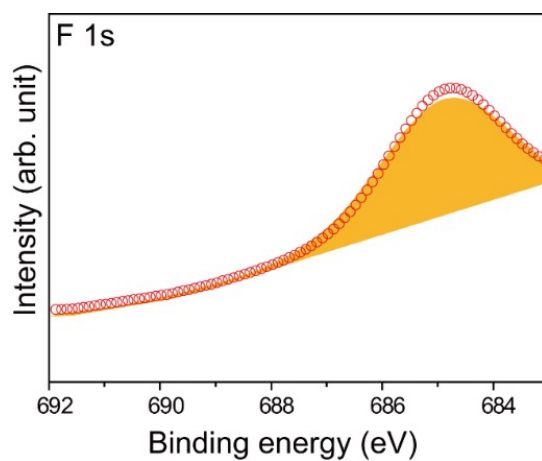**Figure S4.** (a) SEM image and (b) EDX elemental mapping of $Co:C_3N_4$.

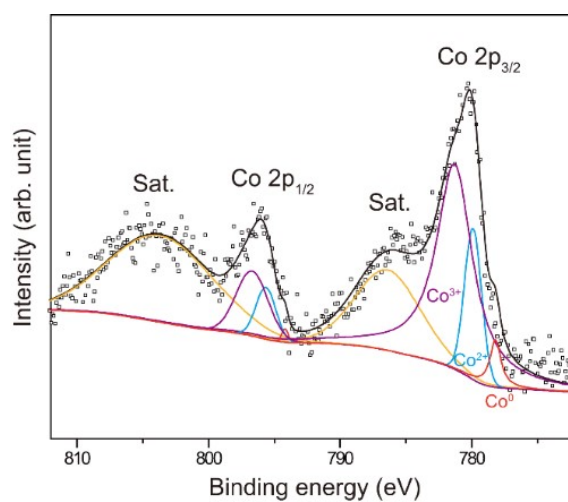**Figure S5.** High resolution F 1*s* XPS spectrum of F:BiVO$_4$.
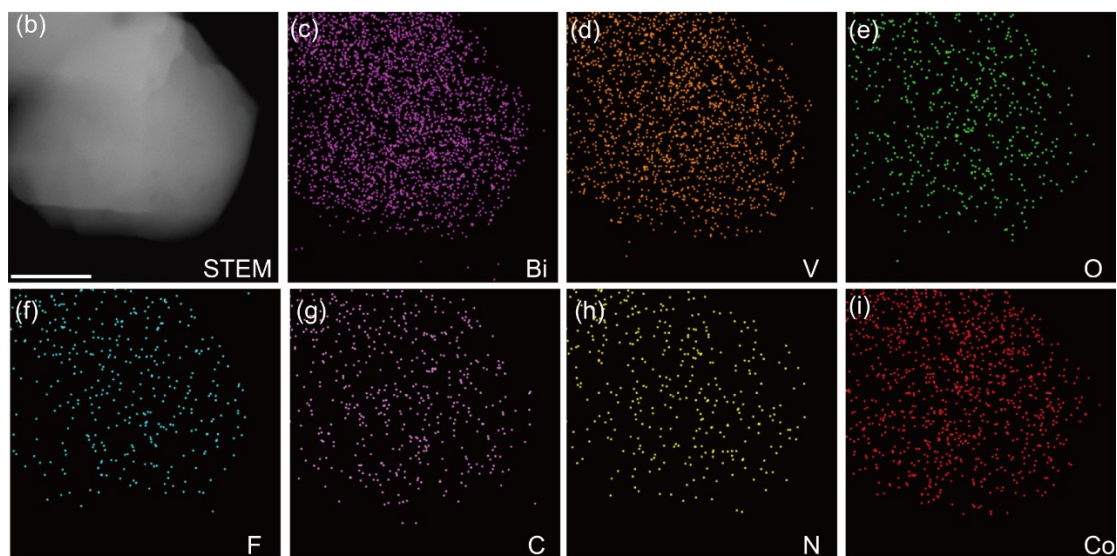

Figure S6. High resolution Co 2*p* XPS spectrum of Co:C$_3$N$_4$.
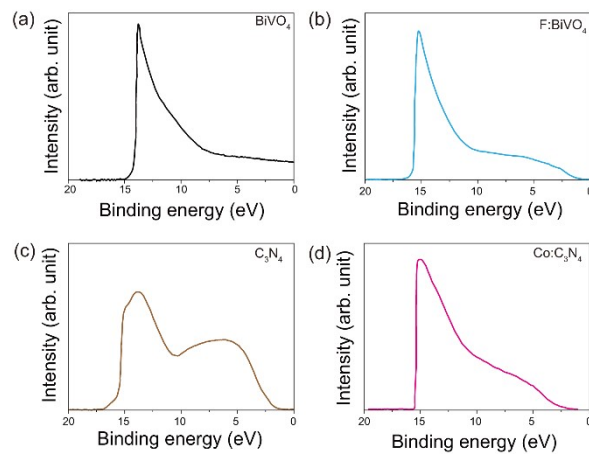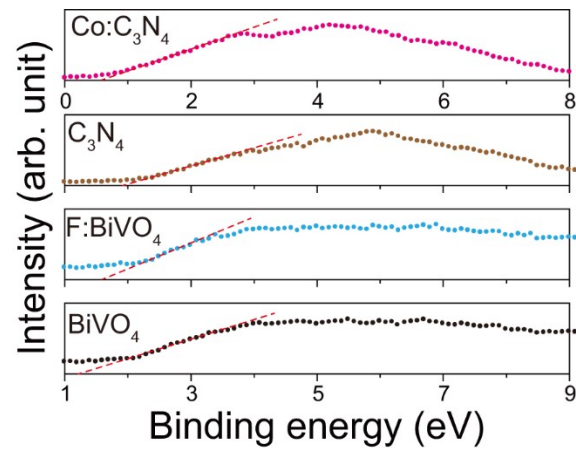

Figure S7. STEM elemental mapping of F:BiVO$_4$/Co:C$_3$N$_4$. (b): STEM image, (c) to (i): Bi, V, O, F, C, N, and Co-elemental mapping, respectively.
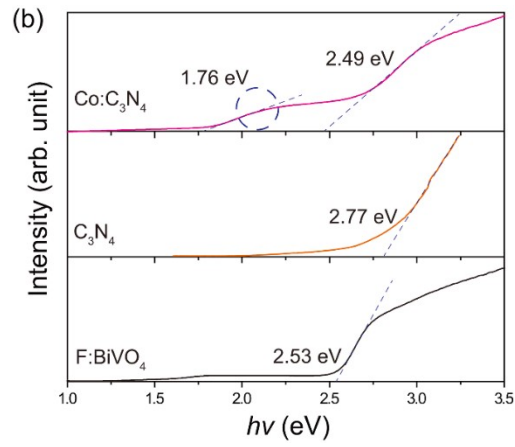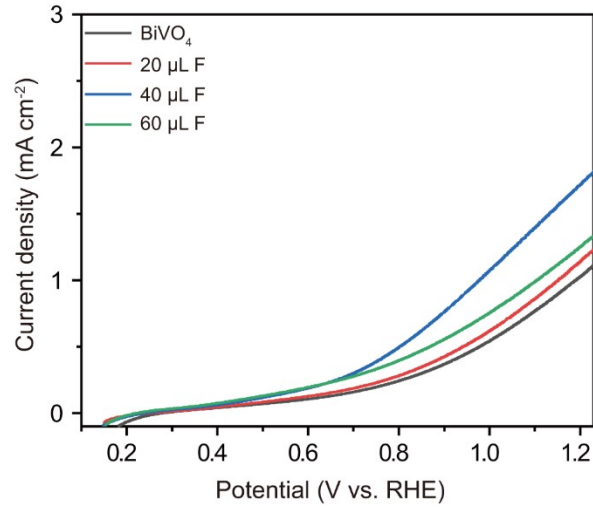
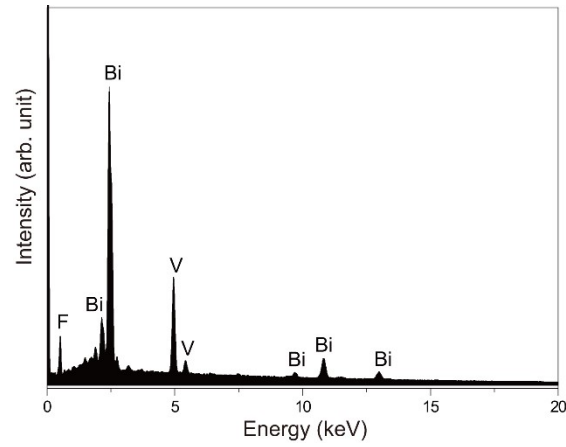**Figure S8.** Tauc-plots of F:BiVO$_4$, C$_3$N$_4$, and Co:C$_3$N$_4$.

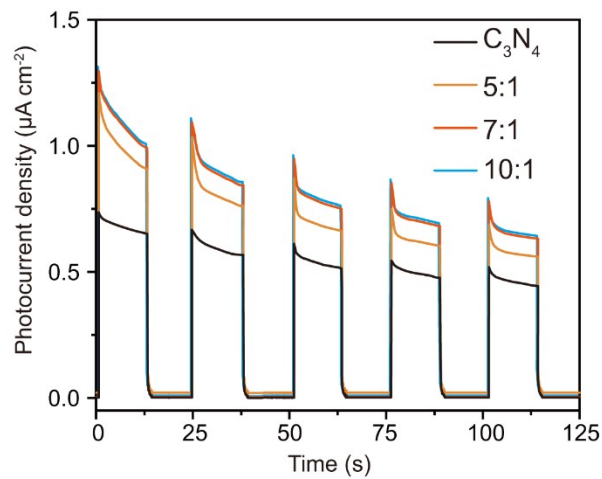**Figure S9.** UPS plots of BiVO$_4$, C$_3$N$_4$, F:BiVO$_4$ and Co:C$_3$N$_4$.

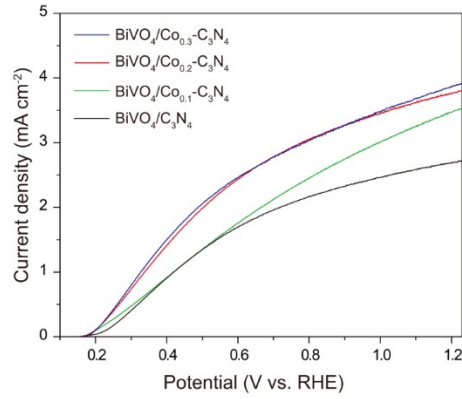**Figure S10.** XPS-valence measurements of BiVO$_4$, C$_3$N$_4$, F:BiVO$_4$ and Co:C$_3$N$_4$.

Figure S11. *J-V* curves of $BiVO_4$ under varied F-doping amount.

**Figure S12.** EDX measurement of $BiVO_4$ with 40 µL F (the optimized one shown in Fig. S11).

**Figure S13.** *I-t* curves of $Co:C_3N_4$ under varied Co-doping amount.

Figure S14. *J-V* curves of $BiVO_4/Co:C_3N_4$ with varied Co contents.

The PEC activity characterizations on $BiVO_4$ coated by C_3N_4 with varied Co single atoms show that Co incorporation increases the PEC activity of $BiVO_4/C_3N_4$, and the photocurrent density increases with the increase of Co content in the precursor for synthesizing $Co:C_3N_4$. Owing to the photocatalytic activity can not be obviously improved beyond the Co content of 6.64 wt.%, we used such Co loading amount for constructing heterojunction.
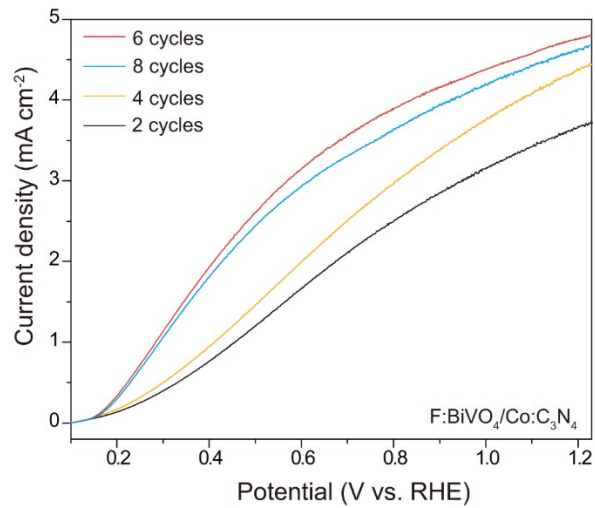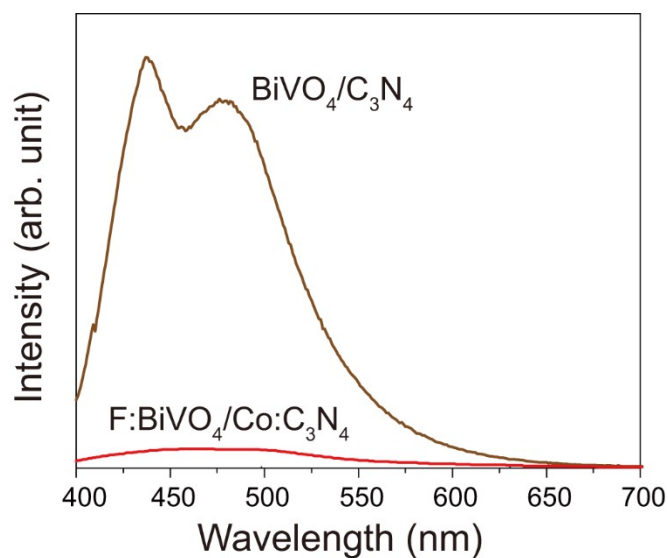

Figure S15. *J-V* curves for $F:BiVO_4/Co:C_3N_4$ sample with varied $Co:C_3N_4$ deposition cycles under illumination.
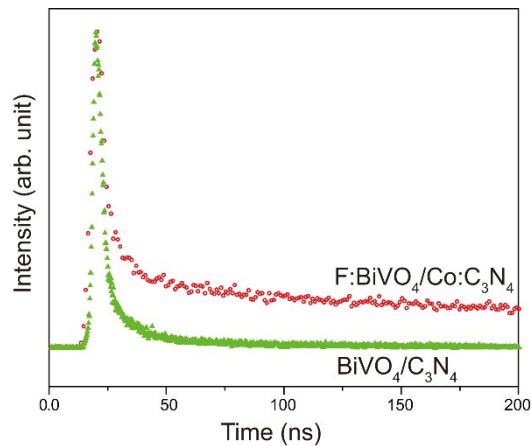
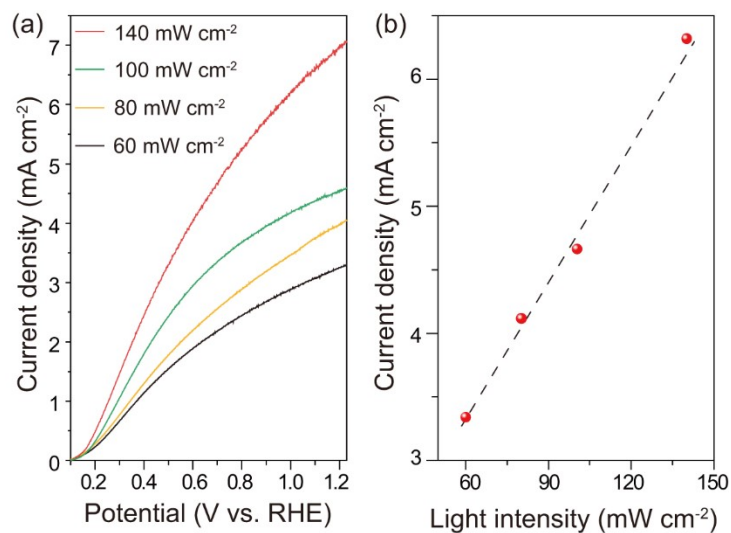
Figure S16. Time-resolved photoluminescence decay curves.

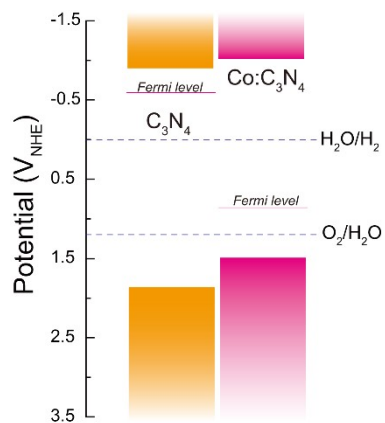**Figure S17.** PL spectra of $BiVO_4$, $BiVO_4/C_3N_4$, $F:BiVO_4/Co:C_3N_4$.

Figure S18. J-V curves for $F:BiVO_4/Co:C_3N_4$ sample under varied light intensity.

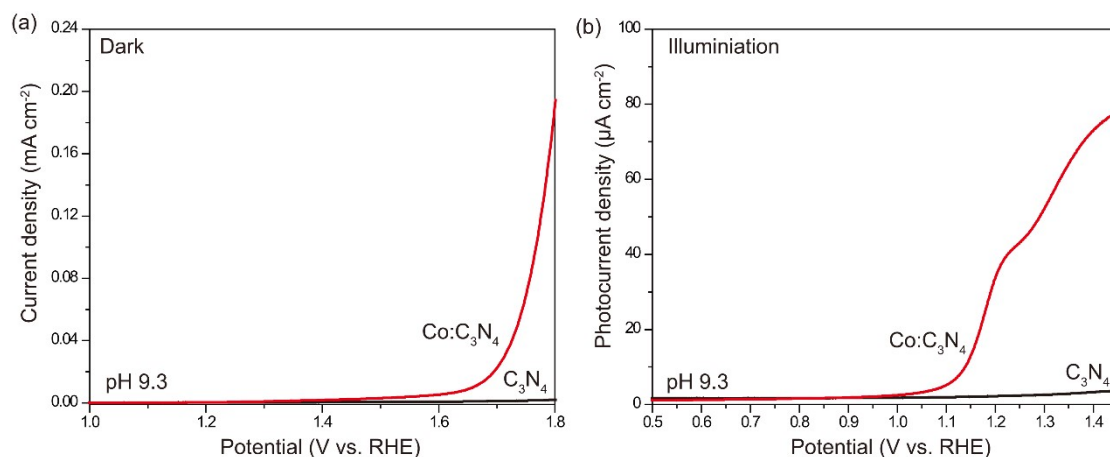**Figure S19.** Measured band structures of C_3N_4 and $Co:C_3N_4$.

Figure S20. (a) LSV curves of rotating disc electrode measurements of C_3N_4 and $Co:C_3N_4$. (b) J-V curves of C_3N_4 and $Co:C_3N_4$ under illumination.
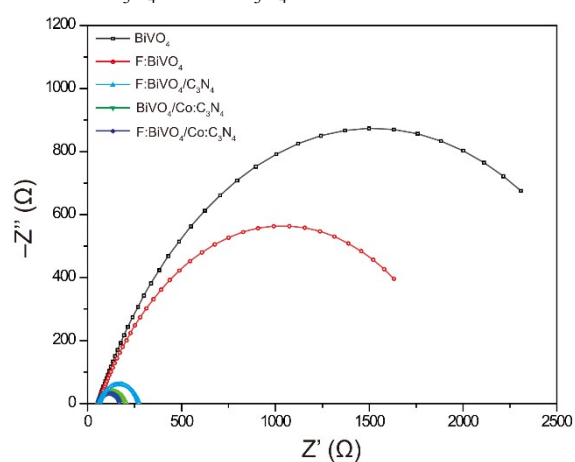
Figure S21. EIS plots of $BiVO_4$, $F:BiVO_4$, $F:BiVO_4/C_3N_4$, $BiVO_4/Co:C_3N_4$ and $F:BiVO_4/Co:C_3N_4$.
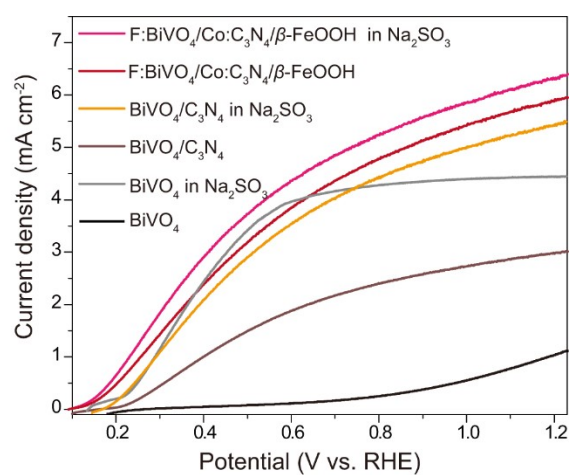
Figure S22. J-V curves of $BiVO_4$, $BiVO_4/C_3N_4$ and $F:BiVO_4/Co:C_3N_4$ photoanodes in 0.5 M KBi electrolyte (pH = 9.3) with/without 0.2 M Na_2SO_3 solution under AM 1.5G simulated sunlight (100 mW cm^{-2}).

Table S1. Co K-edge EXAFS curve fitting results

Samples	Path	CN	R (Å)	σ² (Å²)	ΔE₀ (eV)	R factor

10

Co foil	Co-Co	12	2.50	0.006 ± 0.001	7.9 ± 0.3	0.001
Co:C_3N_4	Co-N	3	2.07	0.007± 0.001	0.4 ± 0.8	0.009

Fitting single scattering for shell 1, while the intensity of Co-Co scattering is too low to fit. CN is the coordination number, R is the interatomic distance, σ^2 is the Debye-Waller factor, ΔE_0 is the edge-energy shift and R-factor is the fitting standard error.

Table S2. ICP-MS result of Co loading amount for Co:C_3N_4.

Sample weight (m_0)	Volume V_0 (mL)	Element	Concentration C_0 (mg/L)	Dilution rate (f)	concentration C_1 (mg/L)	Content (wt.%)
0.0421	10	Co	1.3979	200	279.5790	6.64083%

Table S3. ICP-MS result of Co loading amount for Co:C_3N_4.

Sample weight (m_0)	Volume V_0 (mL)	Element	Concentration C_0 (mg/L)	Dilution rate (f)	concentration C_1 (mg/L)	Content (wt.%)
0.0421	10	Co	1.3979	200	279.5790	6.64083%

Table S4. comparisons on PEC activities of our sample with $BiVO_4$ based heterojunctions reported in literatures.

Photoanode	J (mA cm^{-2} @1.23 V_{RHE})	Electrolyte	References
F:$BiVO_4$/Co:C_3N_4	4.60	0.5M kBi	*This work*
BVO/$BiVO_4$	3.40	0.5 M kBi	*Appl. Catal. B-Environ. 2023, 334, 122865.*
N-CFO/$BiVO_4$	4.83	0.1M kBi	*Appl. Catal. B-Environ. 2023, 320, 121947.*
C_3N_4/$BiVO_4$	4.06	0.5M PBS	*Appl. Surf. Sci. 2020, 523, 146441.*
CNQDs/$BiVO_4$ QDs	2.2	0.05 MNa$_2$SO$_4$	*Next Energy. 2024,1, 100056.*
gC_3N_4/Mo:$BiVO_4$	3.11	0.5M KPi	*J. Power Sources. 2019, 444,227300.*
$BiVO_4$/ C_3N_4	1.14	0.5MNa$_2$SO$_4$	*Chemosphere. 2022, 308, 136166*
FeOOH/Ni-$BiVO_4$	3.02	1M KPi	*J. Colloid Interface Sci. 2023, 604, 162-169.*
$BiVO_4$/In$_2$O$_3$/FeNi	4.0	0.5M Na$_2$SO$_4$	*J. Colloid Interface Sci. 2023, 646, 238-244.*
$BiVO_4$-Co-MOF	2.32	0.5MNa$_2$SO$_4$	*Appl. Surf. Sci. 2023, 619, 156710.*
$BiVO_4$ /Al-CoOOH	3.02	0.5M Na$_2$SO$_4$	ACS Sustainable Chem.Eng. 2023, 11, 13656
$BiVO_4$ /CuPc/FeOOH	3.67	0.5M kBi	*Adv. Mater. Technol. 2023*
$BiVO_4$/NiFe MOF	4.16	0.5M kBi	*J. Colloid Interface Sci. 2024, 654, 1492-1503*
CQDs/Ni(OH)$_2$/$BiVO_4$	3.05	0.2M kBi	*Int. J. Hydrog. Energy. 2023, 48, 36694-36706.*
CoS/$BiVO_4$	3.2	0.5M PBS	*Chin. J. Catal. 2022, 43, 433-441.*

Table S5. Exponential decay-fitted parameters of time-resolved photoluminescence decay curves for $BiVO_4$/C_3N_4 and F:$BiVO_4$/Co:C_3N_4.

Photoanodes	t_1 (ns)	t_2 (ns)	A$_1$ (ns)	A$_2$ (%)	*Lifetime* (ns)
$BiVO_4$/C_3N_4	1.16	18.16	88.74	11.26	12.46
F:$BiVO_4$/Co:C_3N_4	21.66	2.39	29.54	70.46	17.65

Time-resolved photoluminescence decay curves were fitted according to the following equation:

$$Lifetime \text{ (ns)} = \sum_{i=1}^{n} A_i e^{-1/t_i}$$, where n represents the number of exponential curves in fitting and t_i represents the speed of carrier recombination for each exponential curve.

Table S6. Fitted EIS parameters shown in Fig. S21.

R (Ω)	$BiVO_4$	$F:BiVO_4$	$F:BiVO_4/C_3N_4$	$BiVO_4/Co:C_3N_4$	$F:BiVO_4/Co:C_3N_4$
R_s	53.54	56.82	63.48	53.72	57.70
R_{ct}	2932	1963	208	155	112
$CPE_1\text{-}T$	0.00169	0.00024	0.00014	0.00030	0.00015
$CPE_1\text{-}P$	0.6821	0.6648	0.68792	0.58925	0.69648

References

[1] G. Kresse, D. Joubert, *Phys. Rev. B* **1999**, *59*, 1758-1775.

[2] J. P. Perdew, K. Burke, M. Ernzerhof, *Phys. Rev. Lett.* **1996**, *77*, 3865-3868.

[3] H. J. Monkhorst, J. D. Pack, *Phys. Rev. B* **1976**, *13*, 5188-5192.

[4] T. Bucko, S. Lebegue, J. Hafner, J. G. Angyan, *Theory Comput.* **2013**, *9*, 4293.

[5] J. Rossmeisl, A. Logadottir, J. K. Nørskov, *Chem. Phys.* **2005**, *319*, 178-184.

[6] Z. Wang, P. Zhaom Z. Jiang, Y. Lin, J. Zheng, *Phys. B: Condens*. **2023**, 650, 414535